Electronic Supplementary Material (ESI) for ChemComm.
This journal is © The Royal Society of Chemistry 2017

Electronic Supplementary Information

Nucleophilic Reactivity of Copper(II)-Alkylperoxo Complexes†

Bohee Kim, Donghyun Jeong, and Jaeheung Cho*

Department of Emerging Materials Science, DGIST, Daegu 42988, Korea

E-mail: jaeheung@dgist.ac.kr

Experimental Section

Materials and Instrumentation. All chemicals obtained from Aldrich Chemical Co. were the best available purity and used without further purification unless otherwise indicated. The solvents acetonitrile (CH_3CN) and diethyl ether (Et_2O) were passed through solvent purification columns (JC Meyer Solvent Systems) prior to use. ^{18}O Labeled cumene hydroperoxide (95 % ^{18}O-enriched) was prepared by the reported method[S1] and used in cold spray ionization mass spectra (CSI-MS) and resonance Raman studies. The CHDAP (*N*,*N'*-di-cyclohexyl-2,11-diaza[3.3](2,6)-pyridinophane) ligand was prepared by reacting 2,6-bis-(chloromethyl)pyridine with 2,6-bis[(N-cyclohexylamino)methyl]-pyridine at 80 ºC.[S2]

UV-vis spectra were recorded on a Hewlett Packard 8454 diode array spectrophotometer equipped with a UNISOKU Scientific Instruments for low-temperature experiments or with a circulating water bath. Electrospray ionization mass spectra (ESI-MS) were collected on a Waters (Milford, MA, USA) Acquity SQD quadrupole Mass instrument, by infusing samples directly into the source using a manual method. The spray voltage was set at 2.5 kV and the capillary temperature at 80 °C. CSI-MS were collected on a JEOL JMS-T100CS spectrometer. The spray voltage was set at 4.2 kV and the capillary temperature at 80 °C. Resonance Raman spectra were obtained using a liquid nitrogen cooled CCD detector (CCD-1024×256-OPEN-1LS, HORIBA Jobin Yvon) attached to a 1-m single polychromator (MC-100DG, Ritsu Oyo Kogaku) with a 1200 groovs/mm holographic grating. An excitation wavelength of 441.6-nm was provided by a He-Cd laser (Kimmon Koha, IK5651R-G and KR1801C), with 20 mW power at the sample point. All measurements were carried out with a spinning cell (1000 rpm) at −30 ^{o}C. Raman shifts were calibrated with indene, and the accuracy of the peak positions of the Raman bands was ±1 cm^{-1}. The effective magnetic moments were determined using the modified ^{1}H NMR method of Evans at room temperature.[S3-S5] A WILMAD® coaxial insert (sealed capillary) tubes containing the blank acetonitrile-d_3 solvent (with 1.0 % TMS) only was inserted into the normal NMR tubes containing the complexes dissolved in acetonitrile-d_3 (with 0.03 % TMS). The chemical shift of the TMS peak (and/or solvent peak) in the presence of the paramagnetic metal complexes was compared to that of the TMS peak (and/or solvent peak) in the inner coaxial insert tube. The effective magnetic moment was calculated using the equation, $\mu = 0.0618(\Delta vT/2fM)^{1/2}$, where f is the oscillator frequency (MHz) of the superconducting spectrometer, T is the absolute temperature, M is the molar concentration of the metal ion, and Δv is the difference in frequency (Hz) between the two reference signals. EPR spectra were obtained on a JEOL JES-FA200 spectrometer. The EPR spin quantification was carried out using a spin quantification program, JEOL v 2.8.0. v2 series. The spectral simulation was carried out using a simulation software, JEOL AniSimu/FA ver 2.4.0. ^{1}H NMR spectra were measured with Bruker AVANCE III-400 spectrometer at CCRF in DGIST. Crystallographic analysis was conducted with an SMART APEX II CCD equipped with a Mo X-ray tube at CCRF in DGIST. Product analysis was performed with High Performance Liquid

Chromatography (HPLC, Waters Pump Series P580) equipped with a variable wavelength UV-200 detector. Quantitative analysis was made on the basis of comparison of HPLC peak integration between products and authentic samples.

Preparation of Precursor Complexes

[Cu(CHDAP)](ClO_4)$_2$(H_2O) (1-(ClO_4)$_2$(H_2O)). CHDAP (0.18 g, 0.5 mmol) in CH_3CN (2 mL) was added to CH_3CN solution (2 mL) of $Cu(ClO_4)_2{\cdot}6H_2O$ (0.34 g, 0.5 mmol). The mixture was stirred for 12 hours, giving a green solution. Et_2O (40 mL) was added to the resulting solution to yield a green powder, which was collected by filtration, washed with Et_2O, and dried in vacuo. Yield: 0.21 g (60 %). UV-vis in CH_3CN/CH_2Cl_2 (1:1): λ_{max} (ε) = 380 nm (1000 M^{-1} cm^{-1}) and 700 nm (100 M^{-1} cm^{-1}). ESI-MS in CH_3CN (see ESI, Figure S1†): *m/z* 233.7 for $\{Cu(CHDAP)\}^{2+}$, *m/z* 254.2 for $\{Cu(CHDAP)(CH_3CN)\}^{2+}$, and *m/z* 566.2 for $\{Cu(CHDAP)(ClO_4)\}^{+}$. Anal. Calcd for $C_{26}H_{38}CuN_4O_9$: C, 45.58; H, 5.59; N, 8.18. Found: C, 45.55; H, 5.82; N, 8.60. μ_{eff} = 1.79 BM. X-ray crystallographically suitable crystals were obtained by addition of $NaBPh_4$ and slow diffusion of Et_2O into a solution of the complex in CH_3CN.

[Cu(CHDAP)(NO_3)$_2$] (1-(NO_3)$_2$). CHDAP (0.18 g, 0.5 mmol) in CH_3CN (2 mL) was added to CH_3CN solution (2 mL) of $Cu(NO_3)_2$ (0.09 g, 0.5 mmol). The mixture was stirred for 12 hours, giving a green solution. Et_2O (40 mL) was added to the resulting solution to yield a green powder, which was collected by filtration, washed with Et_2O, and dried in vacuo. Yield: 0.22 g (75 %). UV-vis in CH_3CN/CH_2Cl_2 (1:1): λ_{max} (ε) = 370 nm (1100 M^{-1} cm^{-1}) and 760 nm (70 M^{-1} cm^{-1}). ESI-MS in CH_3CN (ESI, Figure S2†):*m/z* 233.7 for $\{Cu(CHDAP)\}^{2+}$, *m/z* 254.2 for $\{Cu(CHDAP)(CH_3CN)\}^{2+}$, and *m/z* 529.4 for $\{Cu(CHDAP)(NO_3)\}^{+}$. Anal. Calcd for $C_{26}H_{36}CuN_6O_6$: C, 52.74; H, 6.13; N, 14.19. Found: C, 52.76; H, 6.12; N, 14.19. μ_{eff} = 1.80 BM. X-ray crystallographically suitable crystals were obtained by slow diffusion of Et_2O into a solution of the complex in CH_3CN.

[Cu(CHDAP)(OOC(CH_3)$_2$Ph)]$^+$ (2)

Treatment of **1** (0.25 mM) with 1 equiv cumene hydroperoxide (cumyl-OOH) in the presence of 1 equiv triethylamine (TEA) in CH_3CN/CH_2Cl_2 (1:1) at –40 ^oC afforded a green solution. $[Cu(CHDAP)(^{18}O^{18}OC(CH_3)_2Ph)]^+$ was prepared by adding 1 equiv cumyl-$^{18}O^{18}OH$ to a solution containing **1** (0.25 mM) and 1 equiv TEA in CH_3CN/CH_2Cl_2 (1:1). UV-vis in CH_3CN/CH_2Cl_2 (1:1): λ_{max} (ε) = 475 nm (1000 M^{-1} cm^{-1}) and 758 nm (70 M^{-1} cm^{-1}). CSI-MS in CH_3CN/CH_2Cl_2 (1:1): *m/z* 618.34 for $\{Cu(CHDAP)(OOC(CH_3)_2Ph)\}^{+}$.

[Cu(CHDAP)(OOBu^t)]$^+$ (3)

Treatment of **1** (0.25 mM) with 1 equiv *tert*-butylhydroperoxide (^{t}BuOOH) in the presence of 1 equiv TEA in CH_3CN/CH_2Cl_2 (1:1) at –40 ^oC afforded a green solution. UV-vis in CH_3CN/CH_2Cl_2 (1:1): λ_{max}

(ε) = 485 nm (850 M^{-1} cm^{-1}) and 763 nm (70 M^{-1} cm^{-1}). CSI-MS in CH_3CN/CH_2Cl_2 (1:1): *m/z* 556.3 for $\{Cu(CHDAP)(OOBu^t)\}^+$.

Characterization of $[Cu(CHDAP)(OOBu^t)]^+$ (3)

The UV-vis spectrum of **3** in CH_3CN/CH_2Cl_2 (1:1) at –40 °C shows two absorption bands at 485 nm (ε = 850 M^{-1} cm^{-1}) and 763 nm (ε = 70 M^{-1} cm^{-1}) (ESI, Figure S5a†), which are similar to those of **2**. The CSI-MS spectrum of **3** exhibits a signal at *m/z* 556.3 (ESI, Figure S5b†), whose mass and isotope distribution pattern correspond to $\{Cu(CHDAP)(OOBu^t)\}$ (calcd *m/z* 556.3). Upon 442 nm excitation at –30 °C, the resonance Raman spectrum of **3** in CH_3CN shows a resonance-enhanced vibrations at 881, 843, 606, 488 and 475 cm^{-1} (ESI, Figure S5a, inset†). These values are comparable to those reported for Cu(II)-*tert*-butylperoxo complex.[S6] The EPR spectrum of a frozen CH_3CN solution of **3** at 113 K shows an axial signal with $g_\perp = 2.05$ and $g_\parallel = 2.26$ ($A_\parallel$ = 140 G), indicating a tetragonal geometry for the Cu(II) ion (ESI, Figure S5c†).[S7] Spin quantification finds that the EPR signal corresponds to 97(2)% of the total copper content in the sample (ESI, Experimental Section†). The similarity of these spectroscopic features to those of **2** leads us to assign **3** as a Cu(II)-*tert*-butylperoxo complex.

X-ray crystallography

Single crystals of $[Cu(CHDAP)(NO_3)_2]$ and $[Cu(CHDAP)(CH_3CN)_2](BPh_4)_2(Et_2O)_2$ were picked from solutions by a nylon loop (Hampton Research Co.) on a hand made copper plate mounted inside a liquid N_2 Dewar vessel at *ca.* –40 °C and mounted on a goniometer head in a N_2 cryostream. Data collections were carried out on a Bruker SMART APEX II CCD diffractometer equipped with a monochromator in the Mo Kα (λ = 0.71073 Å) incident beam. The CCD data were integrated and scaled using the Bruker-SAINT software package, and the structure was solved and refined using SHEXTL V 6.12.[S8] Hydrogen atoms were located in the calculated positions. All non-hydrogen atoms were refined with anisotropic thermal parameters. Crystal data for $[Cu(CHDAP)(NO_3)_2]$: $C_{26}H_{36}CuN_6O_6$, Orthorhombic, $Pna2_1$, $Z = 4$, a = 17.7028(6), b = 9.2443(3), c = 16.1623(6) Å, V = 2644.96(16) $Å^3$, μ = 0.879 mm^{-1}, ρ_{calcd} = 1.487 g/cm^3, R_1 = 0.0404, wR_2 = 0.1239 for 6579 unique reflections, 352 variables. Crystal data for $[Cu(CHDAP)(CH_3CN)_2](BPh_4)_2(Et_2O)_2$: $C_{86}H_{99}B_2CuN_6O_2$, Orthorhombic, *Pbcn*, $Z = 4$, a = 18.9494(12), b = 23.0427(13), c = 17.9917(10) Å, V = 7856.0(8) $Å^3$, μ = 0.327 mm^{-1}, ρ_{calcd} = 1.128 g/cm^3, R_1 = 0.0538, wR_2 = 0.1468 for 7710 unique reflections, 464 variables. The crystallographic data for $[Cu(CHDAP)(NO_3)_2]$ and $[Cu(CHDAP)(CH_3CN)_2](BPh_4)_2(Et_2O)_2$ are listed in Tables S1 and Table S2 lists the selected bond distances and angles. CCDC-1537802 for $[Cu(CHDAP)(NO_3)_2]$ and 1540900 for $[Cu(CHDAP)(CH_3CN)_2](BPh_4)_2(Et_2O)_2$ contain the supplementary crystallographic data for this paper. These data can be obtained free of charge via www.ccdc.cam.ac.uk/data_request/cif (or from the

Cambridge Crystallographic Data Centre, 12, Union Road, Cambridge CB2 1EZ, UK; fax: (+44) 1223-336-033; or deposit@ccdc.cam.ac.uk).

Reactivity studies

All reactions were run in an 1-cm UV cuvette by monitoring UV-vis spectral changes of reaction solutions, and rate constants were determined by fitting the changes in absorbance at 475 nm for $[Cu(CHDAP)(OOC(CH_3)_2Ph)]^+$ (**2**) and 485 nm for $[Cu(CHDAP)(OOBu^t)]^+$ (**3**). Reactions were run at least in triplicate, and the data reported represent the average of these reactions. *In situ*-generated **2** and **3** (0.25 mM) was used in reactivity studies, such as the oxidation of 2-phenylpropionaldehyde (2-PPA) in CH_3CN/CH_2Cl_2 (1:1) at –40 °C (Fig. 2 for **2** and ESI, Fig. S9 for **3**†), and *para*-substituted benzoyl chlorides (*para*-X-Ph-COCl (X = Me, ^{t}Bu, H, Cl, Br)) in CH_3CN/CH_2Cl_2 (1:1) at –40 °C (Fig. 3 for **2** and ESI, Fig. S10 for **3**†). After the completion of reactions, pseudo-first-order fitting of the kinetic data allowed us to determine k_{obs} values. Products formed in the oxidation of 2-PPA by **2** and **3** in CH_3CN/CH_2Cl_2 (1:1) at –40 °C was analyzed by injecting the reaction mixture directly into GC and GC-MS. Products were identified by comparing with authentic samples, and product yields were determined by comparison against standard areas prepared with authentic samples as an internal standard.

Reactivity of $[Cu(CHDAP)(OOBu^t)]^+$ (3)

Upon addition of 2-PPA to **3** in CH_3CN/CH_2Cl_2 (1:1) at –40 °C, similarly, the absorption bands of **3** disappeared with pseudo-first-order decay (ESI, Figure S11a†), and product analysis of the reaction solution revealed that acetophenone (74(6)%) was produced in the oxidation of 2-PPA. **3** is converted to **1** after the reaction was completed. The pseudo-first-order rate constants increased with the substrate concentration, where k_2 (1.8(1) × 10^{-1} M^{-1} s^{-1}) was determined (ESI, Figure S11b†). The activation parameters were determined to be $\Delta H^{\ddagger}$ = 4(1) kJ mol^{-1} and $\Delta S^{\ddagger}$ = –242(3) J mol^{-1} K^{-1} (ESI, Figure S11c†). The Hammett plot of the oxidation of **3** with the *para*-substituted benzoyl chlorides gave the ρ value of 2.1(1) (ESI, Figure S12†), indicating a nucleophilic character of **3**. Product analysis of the final reaction mixture revealed the formation of *para*-substituted benzoic acids.

Computational details

Theoretical calculations were carried out with Density Functional Theory (DFT)[S9] using the Gaussian 09 package.[S10] The B3LYP functional was employed for all geometry optimizations with double-ζ basis sets 6-31G* for all atoms.[S11] All calculations, including the optimizations, were performed in solvent (acetonitile) using the SMD scheme. Optimized geometries were visualized with Gaussview 5. Populations were obtained from a Mulliken Analysis. Molecular orbital compositions and overlap populations between molecular fragments were calculated using the QMForge.[S12] TD-DFT calculations were carried out with the uB3LYP/6-31G* level with 150 roots.[S13] Geometry optimizations were also

performed for 6 coordinated $[Cu(CHDAP)(OOR)(CH_3CN)]^+$ and 5 coordinated $[Cu(CHDAP)(OOR)]^+$ (R = Cumyl or ^{t}Bu). The results show the energy differences of each of two species are 0.3 kcal mol^{-1} for **2** and 2.3 kcal mol^{-1} for **3**, which are in an error range.

References

S1. M. G. Finn, K. B. Sharpless, *J. Am. Chem. Soc.,* 1991, **113**, 113.

S2. J. Kim, B. Shin, H. Kim, J. Lee, J. Kang, S. Yanagisawa, T.Ogura, H. Masuda, T. Ozawa, J. Cho, *Inorg. Chem.,* 2015, **54**, 6176.

S3. D. F. Evans, *J. Chem. Soc*., 1959, 2003.

S4. J. Löliger, R. *J.* Scheffold, *Chem. Educ.,* 1972, **49**, 646.

S5. D. F. Evans, D. A. Jakubovic, *J. Chem. Soc., Dalton Trans.,* 1988, **12**, 2927.

S6. P. Chen, K. Fujisawa, E. I. Solomon, *J. Am. Chem. Soc.*, 2000, **122**, 10177.

S7. T. Fujii, A. Naito, S. Yamaguchi, A. Wada, Y. Funahashi, K. Jitsukawa, S. Nagatomo, T. Kitagawa, H. Masuda, *Chem. Commun.*, 2003, **21**, 2700.

S8. G. M. Sheldrick, *SHELXTL/PC.* Version 6.12 for Windows XP; Bruker AXS Inc.; Madison, WI, 2001.

S9. W. Kohn, L. J. Sham, *Phys. Rev.* 1965, **140**, A1133.

S10. M. J. risch, G. W. rucks, H. B. Schlegel, G. E. Scuseria, M. A. Robb, J. R. Cheeseman, G. Scalmani, V. Barone, B. Mennucci, G. A. Petersson, H. Nakatsuji, M. Caricato, X. Li, H. P. Hratchian, A. F. Izmaylov, J. Bloino, G. Zheng, J. L. Sonnenberg, M. Hada, M. Ehara, K. Toyota, R. Fukuda, J. Hasegawa, M. Ishida, T. Nakajima, Y. Honda, O. Kitao, H. Nakai, T. Vreven, J. A. Montgomery, J. E. Peralta, F. Ogliaro, M. Bearpark, J. J. Heyd, E. Brothers, K. N. Kudin, V. N. Staroverov, R. Kobayashi, J. Normand, K. Raghavachari, A. Rendell, J. C. Burant, S. S. Iyengar, J. Tomasi, M. Cossi, N. Rega, J. M. Millam, M. Klene, J. E. Knox, J. B. Cross, V. Bakken, C. Adamo, J. Jaramillo, R. Gomperts, R. E. Stratmann, O. Yazyev, A. J. Austin, R. Cammi, C. Pomelli, J. W. Ochterski, R. L. Martin, K. Morokuma, V. G. Zakrzewski, G. A. Voth, P. Salvador, J. J. Dannenberg, S. Dapprich, A. D. Daniels, Ö. Farkas, J. B. Foresman, J. V. Ortiz, J. Cioslowski, D. J. Fox, *Gaussian 09, Revision D.01,* Gaussian, Inc., Wallingford CT, 2009.

S11. A. D. Becke, *J. Chem. Phys*., 1993, **98**, 5648.

S12. A. Tenderholt, *Pyspline and QMForge*, 2007.

S13. E. Runge, E. K. U. Gross, *Phys. Rev. Lett*., 1984, **52**, 997.

Table S1. Crystal data and structure refinements for $[Cu(CHDAP)(NO_3)_2]$ (**1**-$(NO_3)_2$) and $[Cu(CHDAP)(CH_3CN)_2](BPh_4)_2(Et_2O)_2$ (**1**-$(CH_3CN)_2(BPh_4)_2(Et_2O)_2$)

	1-$(NO_3)_2$	**1**-$(CH_3CN)_2(BPh_4)_2(Et_2O)_2$
Empirical formula	$C_{26}H_{36}CuN_6O_6$	$C_{86}H_{99}B_2CuN_6O_2$
Formula weight	592.15	1333.87
Temperature (K)	103(2)	143(2)
Wavelength (Å)	0.71073	0.71073
Crystal system/space group	Orthorhombic, $Pna2_1$	Orthorhombic, *Pbcn*
Unit cell dimensions		
a (Å)	17.7028(6)	18.9494(12)
b (Å)	9.2443(3)	23.0427(13)
c (Å)	16.1623(6)	17.9917(10)
α (º)	90.00	90.00
b (Å)	90.00	90.00
γ (º)	90.00	90.00
Volume (Å^3)	2644.96(16)	7856.0(8)
Z	4	4
Calculated density (g/cm^{-3})	1.487	1.128
Absorption coefficient (mm^{-1})	0.879	0.327
Reflections collected	86434	197552
Independent reflections [R(int)]	6579 [0.0568]	7710 [0.1157]
Refinement method	Full-matrix least-squares on F^2	Full-matrix least-squares on F^2
Data/restraints/parameters	6579/1/352	7710/0/464
Goodness-of-fit on F^2	1.163	1.165
Final R indices [$I > 2$sigma(I)]	$R_1 = 0.0404$, $wR_2 = 0.1239$	$R_1 = 0.0538$ $wR_2 = 0.1468$
R indices (all data)	$R_1 = 0.0524$, $wR_2 = 0.1411$	$R_1 = 0.0768$ $wR_2 = 0.1670$

Table S2. Selected bond distances (Å) and angles (º) for [Cu(CHDAP)$(NO_3)_2$] (**1**-$(NO_3)_2$) and [Cu(CHDAP)$(CH_3CN)_2$]$(BPh_4)_2(Et_2O)_2$ (**1**-$(CH_3CN)_2(BPh_4)_2(Et_2O)_2$)

Bond Distances (Å)			
1-$(NO_3)_2$		**1**-$(CH_3CN)_2(BPh_4)_2(Et_2O)_2$	
Cu-O1	2.008(4)	Cu- N1	2.005(2)
Cu-O2	1.977(4)	Cu- N1’	2.005(2)
Cu-N1	2.028(4)	Cu-N2	1.997(2)
Cu-N2	2.382(4)	Cu-N2’	1.997(2)
Cu-N3	2.007(4)	Cu-N3	2.428(2)
Cu-N4	2.408(3)	Cu-N3’	2.428(2)
Bond Angles (°)			
1-$(NO_3)_2$		**1**-$(CH_3CN)_2(BPh_4)_2(Et_2O)_2$	
O1-Cu-O2	81.83(15)	N1-Cu-N1’	89.66(13)
O1-Cu-N1	177.23(15)	N1-Cu-N2	94.00(9)
O1-Cu-N2	98.12(14)	N1-Cu-N2’	171.23(9)
O1-Cu-N3	99.03(15)	N1-Cu-N3	108.38(8)
O1-Cu-N4	103.94(14)	N1-Cu-N3’	92.72(8)
O2-Cu-N1	98.94(15)	N1’-Cu-N2	171.23(8)
O2-Cu-N2	109.35(14)	N1’-Cu-N2’	94.00(9)
O2-Cu-N3	171.26(16)	N1’-Cu-N3	97.72(8)
O2-Cu-N4	92.78(14)	N1’-Cu-N3’	108.38(8)
N1-Cu-N2	79.12(14)	N2-Cu-N2’	83.52(12)
N1-Cu-N3	80.62(15)	N2-Cu-N3	78.56(8)
N1-Cu-N4	78.70(14)	N2-Cu-N3’	79.44(8)
N2-Cu-N3	79.20(14)	N2’-Cu-N3	79.44(8)
N2-Cu-N4	150.73(13)	N2’-Cu-N3’	78.57(8)
N3-Cu-N4	78.55(14)	N3-Cu-N3’	150.36(11)

Table S3. Selected bond distances (Å) from the obtained crystal structure and the DFT calculations of $[Cu(CHDAP)(CH_3CN)_2]^{2+}$ (**1**-$(CH_3CN)_2$), $[Cu(CHDAP)(OOC(CH_3)_2Ph)]^+$ (**2**) and $[Cu(CHDAP)(OOBu^t)]^+$ (**3**)

	1-$(CH_3CN)_2$ (exp.)	**1**-$(CH_3CN)_2$ (cal.)	**2**	**3**
Cu-N_{eq}	2.001(2)	2.00	2.06	2.05
Cu-N_{axial}	2.428(2)	2.44	2.48	2.46
Cu-O			1.89	1.89
O-O			1.46	1.47

Table S4. Mulliken spin density distribution of $[Cu(CHDAP)(OOC(CH_3)_2Ph)]^+$ (**2**)

Orbital	Cu	O_{inner}	O_{outer}	Cumyl	CHDAP
β-HOMO	0.07	0.51	0.30	0.05	0.09
β-LUMO	0.67	0.11	0.01	0.01	0.34

Table S5. Catalytic oxidative reaction of [Cu(CHDAP)$(NO_3)_2$] (**1**-$(NO_3)_2$) and 100 equiv of substrate in the presence of 2 equiv of triethylamine (TEA) and excess amount of alkylperoxides in CH_3CN/CH_2Cl_2 (1:1) at 25 ºC during 1h

alkylperoxide	substrate	product	TON
cumylhydroperoxide	xanthene	xanthone	11(1)
	dihydroanthracene	anthracene	6(1)
	cyclohexadiene	benzene	10(1)
tert-butylhydroperoxide	xanthene	xanthone	2(1)
	dihydroanthracene	anthracene	3(1)
	cyclohexadiene	benzene	6(1)

[substrate] = 25 mM, [alkylperoxides] = 25 mM, [TEA] = 0.5 mM, [catalyst] = 0.25 mM. Turnover number = [product]/[catalyst].

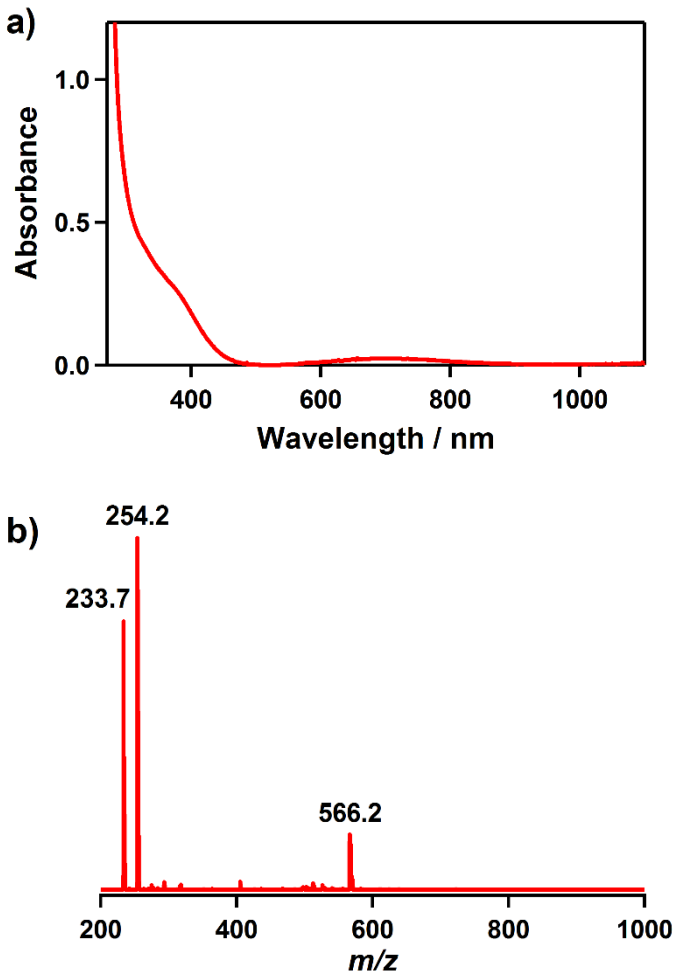

Figure S1. (a) UV−vis spectrum of $[Cu(CHDAP)](ClO_4)_2(H_2O)$ (**1**-$(ClO_4)_2{\cdot}H_2O$) in CH_3CN/CH_2Cl_2 (1:1) at −40 °C. (b) ESI-MS spectrum of **1**-$(ClO_4)_2{\cdot}H_2O$ in CH_3CN/CH_2Cl_2 (1:1). Mass peaks at 233.7, 254.2 and 566.2 are assigned to $\{Cu(CHDAP)\}^{2+}$, $\{Cu(CHDAP)(CH_3CN)\}^{2+}$ and $\{Cu(CHDAP)(ClO_4)\}^{+}$, respectively.

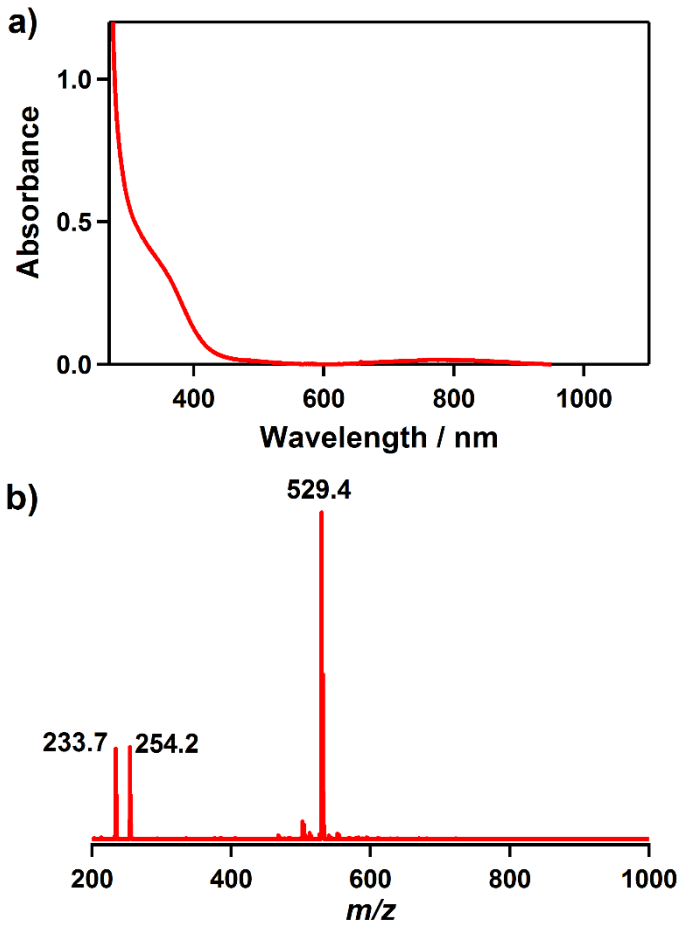

Figure S2. (a) UV−vis spectrum of $[Cu(CHDAP)(NO_3)_2]$ (**1**-$(NO_3)_2$) in CH_3CN/CH_2Cl_2 (1:1) at –40 °C. (b) ESI-MS spectrum of **1**-$(NO_3)_2$ in CH_3CN/CH_2Cl_2 (1:1). Mass peaks at 233.7, 254.2 and 529.4 are assigned to $\{Cu(CHDAP)\}^{2+}$, $\{Cu(CHDAP)(CH_3CN)\}^{2+}$ and $\{Cu(CHDAP)(NO_3)\}^{+}$, respectively.

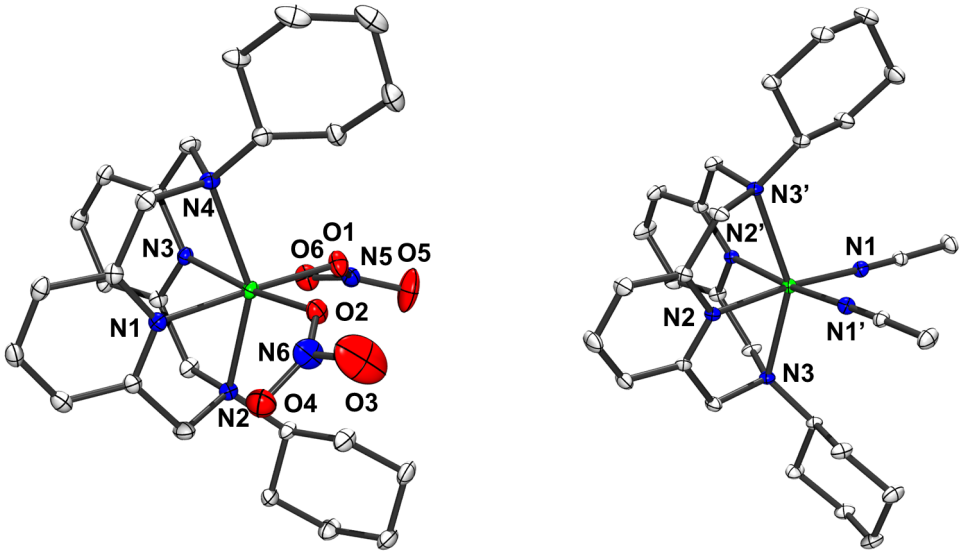

Figure S3. X-ray crystal structures of the $[Cu(CHDAP)(NO_3)_2]$ (**1**-$(NO_3)_2$) (left) and $[Cu(CHDAP)(CH_3CN)_2]^{2+}$ (**1**-$(CH_3CN)_2$) (right) with thermal ellipsoids drawn at the 30% probability level. Hydrogen atoms are omitted for clarity.

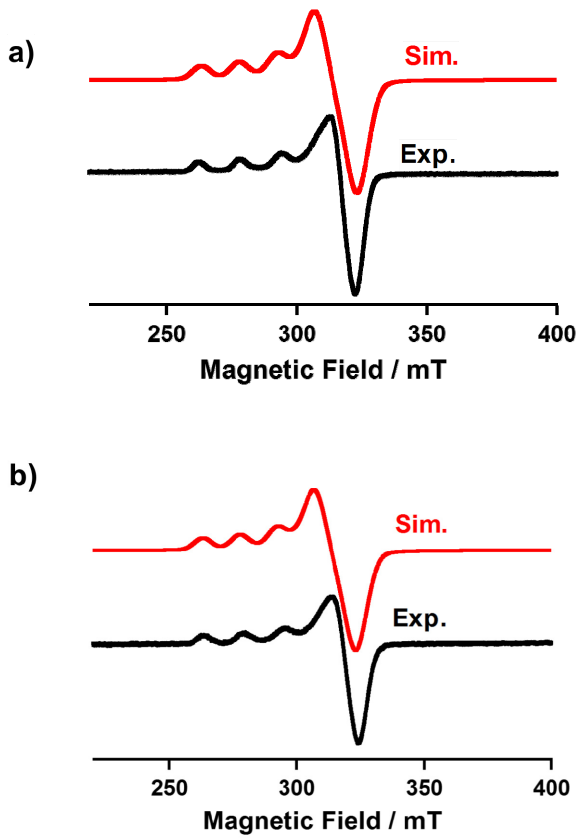

Figure S4. X-band EPR spectrum (black line) and simulation (red line) of (a) $[Cu(CHDAP)(NO_3)_2]$ (**1**-$(NO_3)_2$) ($g_{\parallel}$ = 2.30, $g_{\perp}$ = 2.07 and $A_{\parallel}$ = 171 G) and (b) $[Cu(CHDAP)(CH_3CN)_2](BPh_4)_2(Et_2O)_2$ (**1**-$(CH_3CN)_2(BPh_4)_2(Et_2O)_2$) ($g_{\parallel}$ = 2.28, $g_{\perp}$ 2.06 and $A_{\parallel}$ = 167 G) in frozen CH_3CN at 113 K. Instrumental parameters: microwave power = 0.998 mW, frequency = 9.16 GHz, sweep width = 0.2 T, modulation amplitude = 0.6 mT.

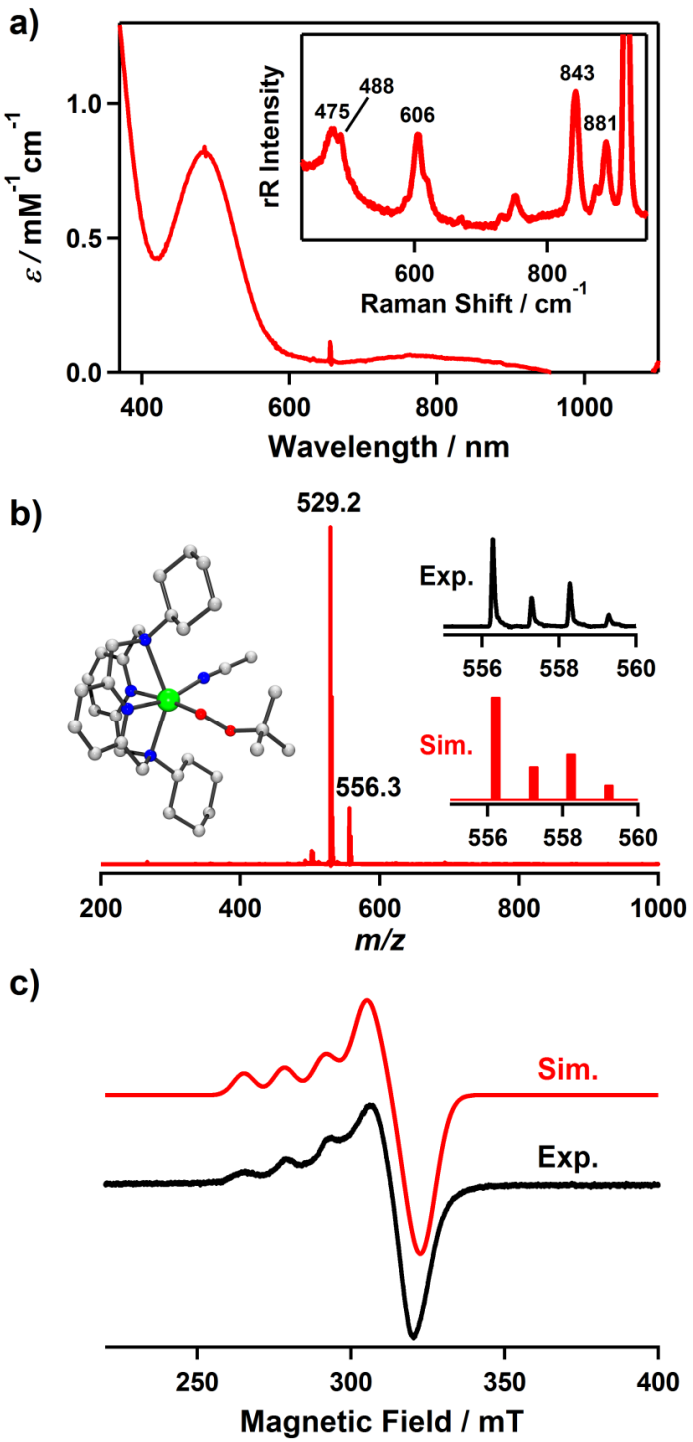

Figure S5. (a) UV−vis spectrum of $[Cu(CHDAP)(OOBu^t)]^+$ (**3**) in CH_3CN/ CH_2Cl_2 (1:1) and at –40 °C. The inset shows the Resonance Raman spectra of **3** (16 mM) obtained upon excitation at 442 nm in CH_3CN at −30 °C. (b) CSI-MS of **3** in CH_3CN/CH_2Cl_2 (1:1) at –40 °C. Mass peaks at 529.2 and 556.3 are assigned to $\{Cu(CHDAP)(NO_3)\}^+$ and $\{Cu(CHDAP)(OOBu^t)\}^+$, respectively. The left inset shows DFT-calculated structure of **3** (gray, C; blue, N; red, O; green Cu). (c) X-band EPR spectrum (black line) and simulation (red line) of **3** (g = 2.26 and 2.05) in frozen CH_3CN at 113 K. Instrumental parameters: microwave power = 0.998 mW, frequency = 9.18 GHz, sweep width = 0.2 T, modulation amplitude = 0.6 mT.

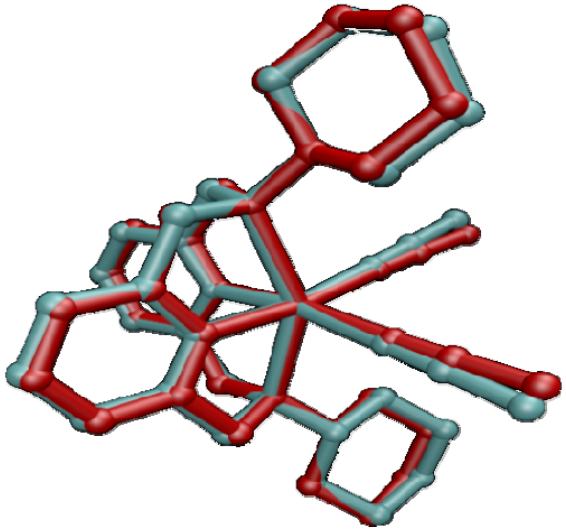

Figure S6. An overlay of the crystal (blue) and calculated (red) structures of $[Cu(CHDAP)(CH_3CN)_2]^{2+}$ (**1**-$(CH_3CN)_2$). The calculated RMS deviation is 0.21 Å.

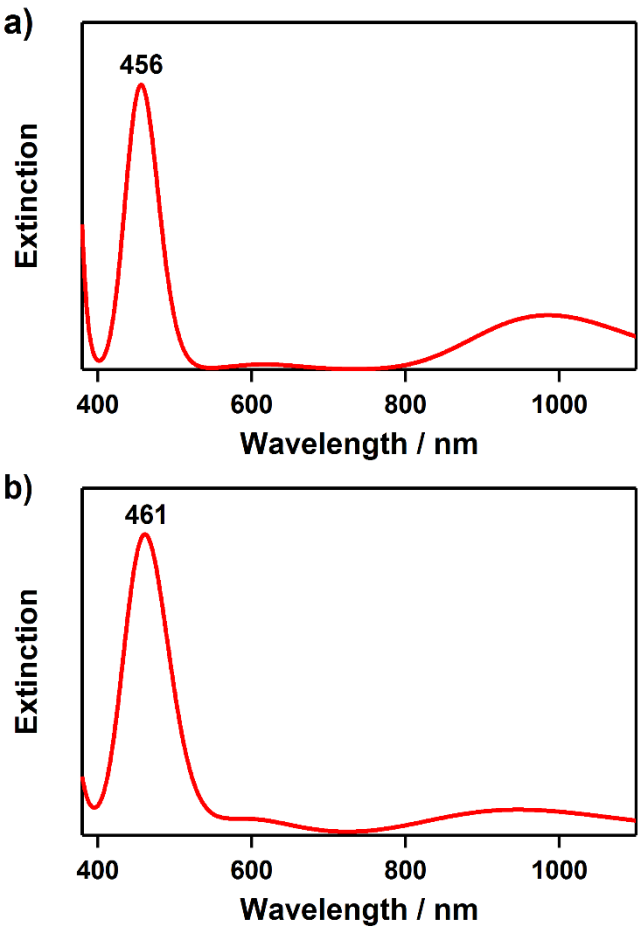

Figure S7. TD-DFT predicted absorption spectra of (a) $[Cu(CHDAP)(OOC(CH_3)_2Ph)]^+$ (**2**) and (b) $[Cu(CHDAP)(OOBu^t)]^+$ (**3**).

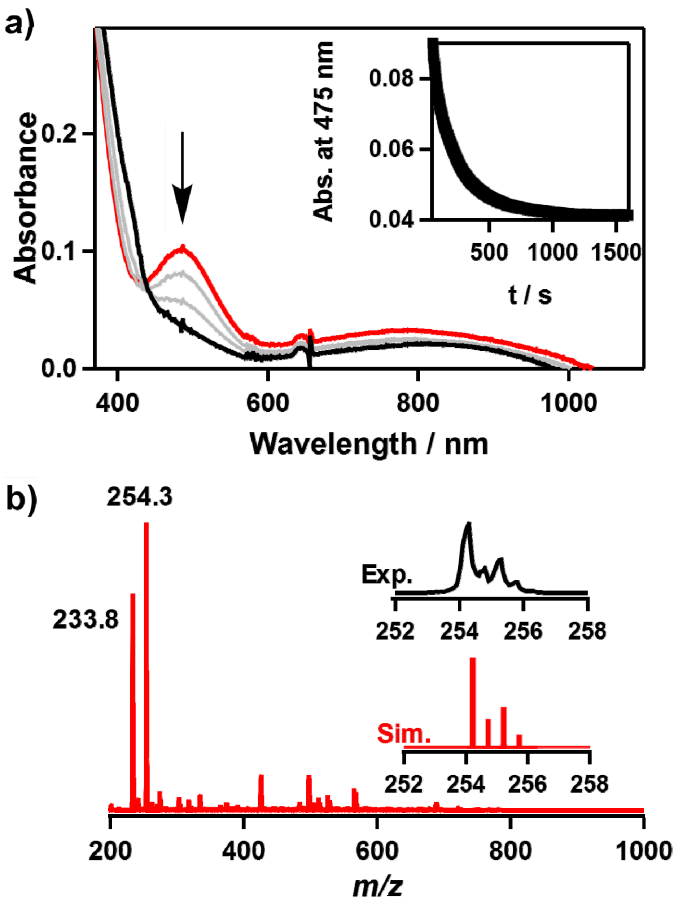

Figure S8. (a) UV−vis spectral changes observed upon natural decay of $[Cu(CHDAP)(OOC(CH_3)_2Ph)]^+$ (**2**) (0.25 mM) in CH_3CN/CH_2Cl_2 (1:1) at 25 °C. The inset shows the time course of the absorbance at 475 nm. (b) ESI-MS taken after natural decay of **2** in CH_3CN/CH_2Cl_2 (1:1) at 25 °C, showing the formation of a Cu(II) precursor: Mass peaks at *m/z* of 233.8 and 254.3 are assigned to $\{Cu(CHDAP)\}^{2+}$ and $\{Cu(CHDAP)(CH_3CN)\}^{2+}$, respectively.

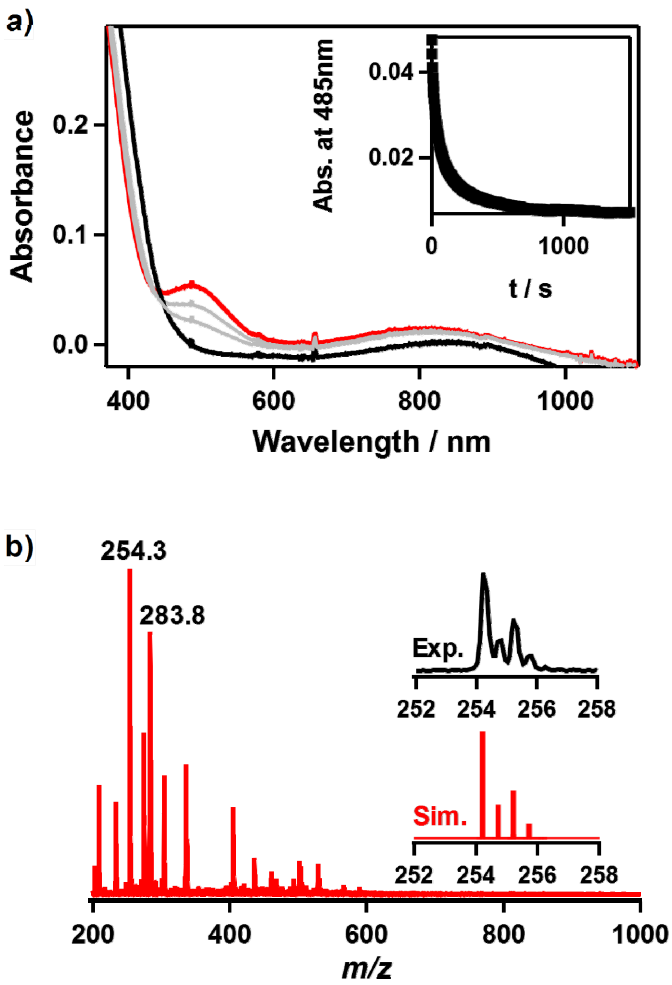

Figure S9. (a) UV−vis spectral changes observed upon natural decay of $[Cu(CHDAP)(OOBu^t)]^+$ (**3**) (0.25 mM) in CH_3CN/CH_2Cl_2 (1:1) at 25 °C. The inset shows the time course of the absorbance at 485 nm. (b) ESI-MS taken after natural decay of **3** in CH_3CN/CH_2Cl_2 (1:1) at 25 °C, showing the formation of a Cu(II) precursor together with unidentified species: Mass peaks at *m/z* of 254.3 and 283.8 are assigned to $\{Cu(CHDAP)(CH_3CN)\}^{2+}$ and $\{Cu(CHDAP)(CH_3CN)_2(H_2O)\}^{2+}$, respectively.

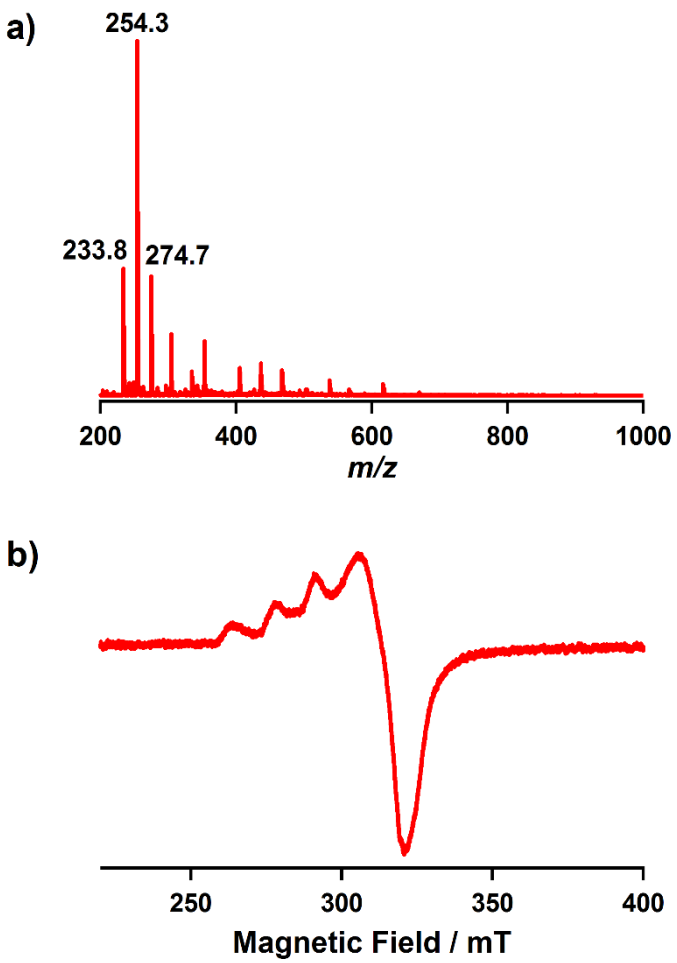

Figure S10. (a) ESI-MS taken after the completion of the reaction of $[Cu(CHDAP)(OOC(CH_3)_2Ph)]^+$ (**2**) with 2-PPA in CH_3CN/CH_2Cl_2 (1:1) at –40 °C, showing the formation of a Cu(II) precursor: Mass peaks at *m/z* of 233.8, 254.3 and 274.7 are assigned to $\{Cu(CHDAP)\}^{2+}$, $\{Cu(CHDAP)(CH_3CN)\}^{2+}$ and $\{Cu(CHDAP)(CH_3CN)_2\}^{2+}$, respectively. (b) X-band EPR spectrum taken after the completion of the reaction of **2** with 2-PPA in CH_3CN/CH_2Cl_2 (1:1) at –40 °C (g = 2.30 and 2.07) in frozen CH_3CN/CH_2Cl_2 (1:1) at 113 K. Instrumental parameters: microwave power = 0.998 mW, frequency = 9.16 GHz, sweep width = 0.25 T, modulation amplitude = 0.6 mT.

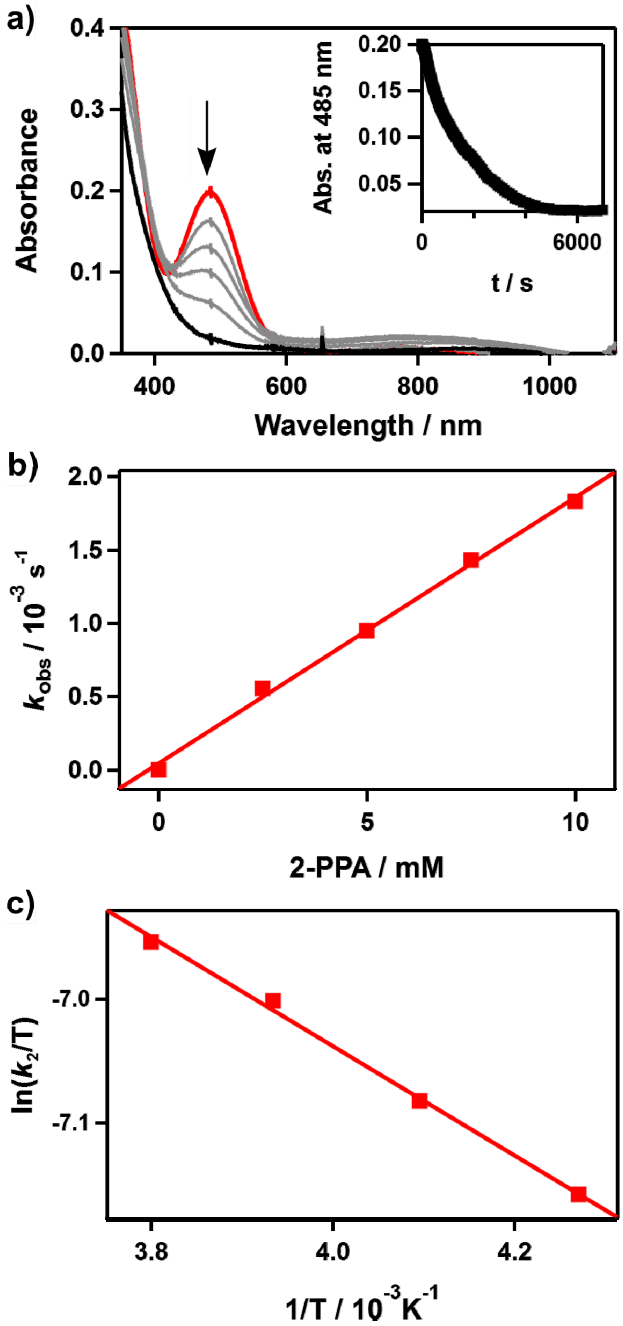

Figure S11. Reactions of $[Cu(CHDAP)(OOBu^t)]^+$ (**3**) with 2-phenylpropionaldehyde (2-PPA) in CH_3CN/CH_2Cl_2 (1:1). (a) UV-vis spectral changes of **3** (0.25 mM) upon addition of 10 equiv of 2-PPA at –40 °C. Inset shows the time course of the absorbance at 485 nm. (b) Plot of k_{obs} against 2-PPA concentration to determine a second-order rate constant. (c) Plot of second-order rate constants against $1/T$ to determine activation parameters.

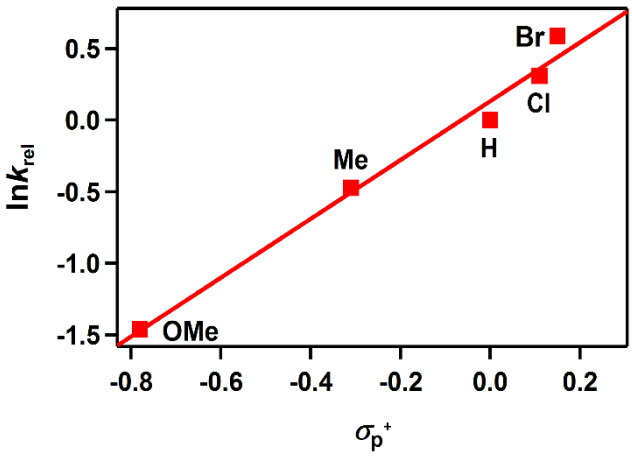

Figure S12. Hammett plot of $\ln k_{rel}$ against σ_p^+ of benzoyl chloride derivatives in the reaction of $[Cu(CHDAP)(OOBu^t)]^+$ (**3**) (0.25 mM) with *para*-substituted benzoyl chloride. The k_{rel} values were calculated by dividing k_{obs} of *para*-X-Ph-COCl (X = OMe, Me, H, Cl, Br) by k_{obs} of benzoyl chlorides in CH_3CN/CH_2Cl_2 (1:1) at –40 °C.